EFFECT OF HIGH PRESSURE TORSION ON THE STRUCTURE, MICROHARDNESS AND HEATING BEHAVIOUR OF THE MAGNESIUM ALLOY WE43

ВЛИЯНИЕ КРУЧЕНИЯ ПОД ВЫСОКИМ ДАВЛЕНИЕМ НА СТРУКТУРУ, МИКРОТВЕРДОСТЬ И ПОВЕДЕНИЕ ПРИ НАГРЕВЕ МАГНИЕВОГО СПЛАВА WE43

PhD Lukyanova E.A.[1,2], PhD student Martynenko N.S.[1,2], PhD Li E.V.[1], PhD Serebryany V.N.[2],
Prof., Dr. Sci. Belyakov A.N.[3], Prof. Dr. Sci. Rokhlin L.L.[2], Prof. Dr. Sci. Dobatkin S.V.[1,2], Prof. Estrin Yu.Z.[1,4]
[1]National University of Science and Technology "MISIS", Laboratory of Hybrid Nanostructured Materials, Moscow, Russia
[2]A.A. Baikov Institute of Metallurgy and Materials Science of Russian Academy of Sciences, Moscow, Russia
[3]Belgorod State University, Belgorod, Russia
[4]Department of Materials Engineering, Monash University, Clayton, VIC 3800, Australia
E-mail: helenelukyanova@gmail.com, nataliasmartynenko@gmail.com, li_elina2787@mail.ru, vns@imet.ac.ru, belyakov@bsu.edu.ru, rokhlin@imet.ac.ru, dobatkin.sergey@gmail.com, yuri.estrin@monash.edu

Abstract: *In the present work, the magnesium alloy WE43 (Mg-Y-Nd-Zr) after high pressure torsion (HPT) was investigated. HPT was conducted at room temperature, 200 °C or 300 °C. As a result of HPT processing, a large number of twins with the twin size of 0.4 − 8.1 μm were formed. Furthermore, the HPT process led to the formation of a very fine grain structure with the average grain size of 30 - 100 nm. The deformation by HPT caused the formation of a displaced basal texture, which sharpens with an increase in the deformation temperature. The refinement of the microstructure brought about an improvement of the microhardness of the alloy over the as-received condition. The microhardness after HPT at the room temperature increased up to 1189 ± 33MPa compared with 774 ± 50 MPa in the initial state. A subsequent aging after HPT led to an additional strengthening to a level of 1411 ± 40 MPa. It was noted that thermal stability of strengthening caused by HPT did not depend on the deformation temperature and sustained up to 250 °C.*

KEYWORDS*: MAGNESIUM ALLOYS, HIGH PRESSURE TORSION, NANOCRYSTALLINE MATERIALS, MICROHARDNESS, AGE HARDENING, STRUCTURE, TEXTURE*

1. Introduction

Nowadays, magnesium alloys are becoming more attractive as materials for biodegradable implant applications owing to their good mechanical properties and biocompatibility [1-3]. Magnesium alloy WE43 is one of the most popular Mg alloys for medical applications. This alloy has a good corrosion resistance, but it is necessary to improve its mechanical properties. It is well known that severe plastic deformation (SPD) can enable the formation of a very fine structure, which gives an increase in strength. There are several methods of SPD. Among the methods of SPD, equal channel angular pressing (ECAP) [4-6] and friction stir processing [7-9] were tested on the WE43 alloy. High pressure torsion (HPT) is one the most popular of SPD methods, which allows to investigate the microstructure evolution in case of high degrees of deformation and simulate hardening processes [10]. It is well known that HPT allows to obtain a grain structure in the submicron or nanoscale range. Analysis of the literature showed that HPT treatment is successfully used for refinement of the structure of pure magnesium and its alloys [11-14] to obtain structures with an average grain size of about 100 nm. HPT was also used for the WE43 alloy [15, 16], but, in general, only the structure after deformation and the subsequent aging process were studied. The purpose of this work is to study the effect of HPT on the structure, distribution of microhardness, texture and behavior during heating of the alloy WE43.

2. Materials and Methods

In this paper, the homogenized at a temperature of 525 °C for 8 hours WE43 alloy (Mg–3.56%Y–2.20%Nd–0.47%Zr) was obtained by HPT at room temperature, 200 °C and 300 °C. For this purpose, samples with a diameter of 20 mm and a thickness of 1.5 mm were deformed with 1 rpm rotation speed under 6 GPa pressure for 10 revolutions (a true strain on the half-radius of the disk was ε=5.7). To study the thermal stability the alloy after deformation was heated in the temperature range 100-400°C with a step of temperature change 50 °C. A study of the kinetics of aging was carried out during heating of the alloy samples at 200 °C with a gradually increasing heating time. The microhardness was measured on a 402 MVD Instron Wolpert Wilson Instruments tester with a load of 50 g and 10 s holding time. The resistivity was measured using a BSZ-010-2 microhmmeter on the flat samples of 18×6×0.9 mm in size. The microstructures were observed using an optical microscope Reichert MeF and transmission electron microscope (TEM) Jeol JEM 2100 operating at 200 kV.

Texture analysis was carried out using X-ray diffraction in a DRON-7 goniometer with the CuKα radiation in the reflection mode. Five incomplete pole figures, {00.4}, {21.1}, {10.2}, {10.3}, {11.0} were obtained with a step of 5° in the radial angle α and the azimuth angle β (0-360°) on a pole figure (α and β – radial and azimuth angles on the pole figure, maximum inclination angle α_{max}=70°).

3. Results and Discussion

Fig. 1 shows the microhardness distribution maps with an area of 13x13 mm^2 inscribed in a sample with a diameter of 20 mm for samples after HPT at 200 °C (Fig. 1a) and after the same treatment, but with subsequent aging at 200 °C for 2 hours (Fig.1b). It can be seen that the microhardness has the maximum values at the edges of the sample and gradually decreases approaching the center. Such a distribution of the microhardness along the diameter of the sample correlates with the dependence of the shear strain on the radius (rate of strain linearly increases along the radius of the specimen from the center to the edge). It can be seen that aging at 200 °C leads to an additional increase in microhardness, which is distributed as a function of the radius qualitatively similar way. So, according to Fig. 1 the microhardness values have the minimum at the center of the sample and the maximum at the edge of the sample, but on the middle of the radius the values of HV are close to the values at the edge. Thereby, all subsequent measurements of the microhardness were performed at the middle of the radius of the sample.

The results of measuring the microhardness of the WE43 alloy in the middle of the sample radius showed that HPT at all deformation temperatures leads to its significant hardening compared with the initial homogenized state. The average microhardness of the alloy samples were as follows: after homogenization – 774 ± 50 MPa, after HPT at room temperature – 1189 ± 33 MPa, after HPT at 200°C and 300°C – 1144 ± 23 MPa and 1118 ± 21 MPa, respectively.

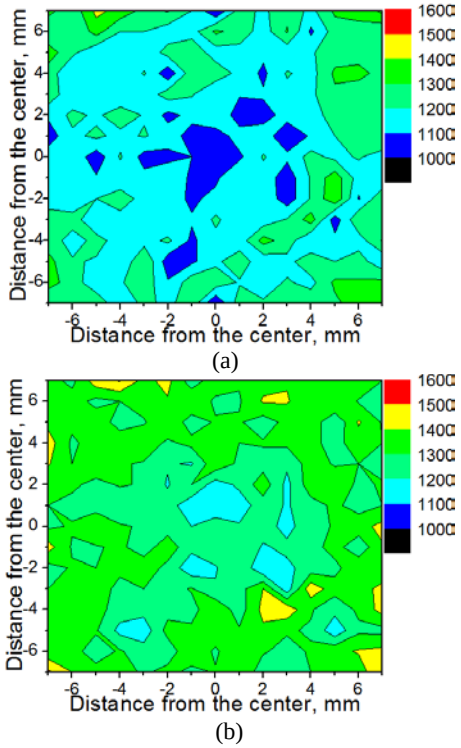

Fig. 1. Maps of microhardness distribution over the surface of samples of WE43 alloy after HPT at 200 °C (a) and after HPT at 200 °C + aging at 200 °C for 2 hours (b).

The change of microhardness and electrical resistivity of alloy samples after both homogenization and HPT at different deformation temperatures as a function of the heating temperature is shown in Fig. 2.

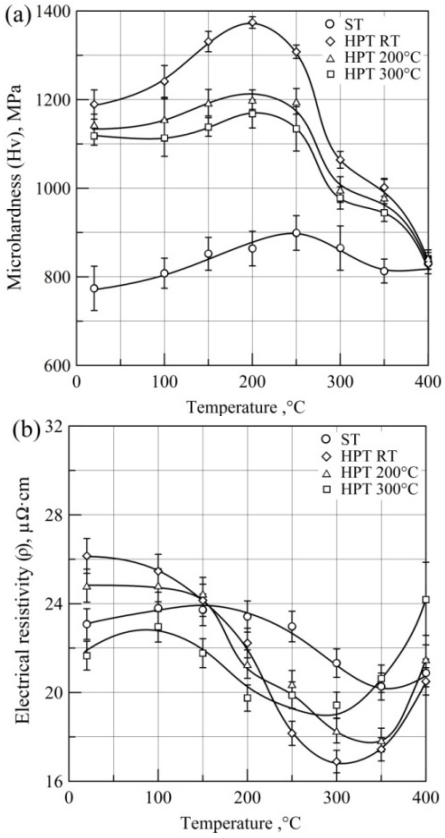

Fig. 2. Microhardness (a) and electrical resistivity (b) of the WE43 alloy as function of annealing temperature.

The microhardness of the WE43 alloy after the HPT at all deformation temperatures is much higher than in the initial state. At the same time, the highest values of microhardness are achieved after HPT at room temperature (Fig. 2a). It can be seen that the curves of microhardness changing have a maximum at 200 °C for alloy after HPT and at 250 °C for alloy in initial state. Herewith, the microhardness growth is greatest for the sample after the HPT at room temperature. Apparently, precipitation of hardening metastable phases at given temperatures caused by the growth of microhardness [17]. This can be confirmed by a decrease in the electrical resistivity in this temperature range, which indicates a depletion of the magnesium solid solution (Fig. 2b). With a further increase in the temperature, the microhardness decreases, until the initial microhardness level of the homogenized state is reached. The solidification of the alloy with an increase in the heating temperature can be caused by the growth of grains and the dissolution of phase, which are rich in rare earth metals and formed in the previous stage of heating. This is also confirmed by the growth of the electrical resistivity at elevated temperatures.

The change of microhardness and electrical resistivity of alloy samples as a function of the duration of isothermal aging at 200 °C is shown in Fig. 3 a,b.

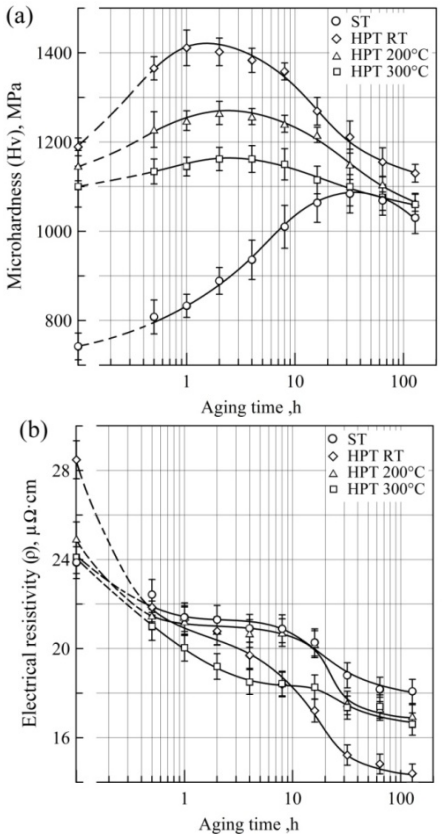

Fig. 3. Microhardness (a) and electrical resistivity (b) of the WE43 alloy as a function of aging time during isothermal aging at 200 °C.

With an increase in the heating time, the microhardness increases for all four alloy states of the alloy, but the greatest increase is observed for HPT at room temperature (Fig. 3a). Moreover, it was noted that the maximum of microhardness of the alloy after HPT is achieved much faster than for the undeformed state.

The maximum of microhardness for the sample after HPT at room temperature (1411 ± 40 MPa) is already reached after aging for 1 h, after HPT at 200 °C (1265 ± 26 MPa) – for 2 hours, after HPT at 300 °C (1162 ± 30 MPa) – for 2-4 hours and, finally, for undeformed sample (1084 ± 43 MPa) – for 32 hours. Hardening during aging is probably caused by the precipitation of hardening metastable phases, as indicated by a decrease in the electrical resistivity (Fig. 3b). From the fact that the electrical resistivity decreases more acutely for the sample after the HPT at room temperature and less for the homogenized state, it can be concluded that the deformation induced by the HPT promotes an increase in the rate of decomposition of the supersaturated solid solution, which causes a reduction in the aging time to reach the maximum microhardness. The acceleration of the decomposition of a supersaturated solid solution based on magnesium in an alloy produced by HPT can be associated with the rapid nucleation and growth of phase particles because of the high density of dislocations and the branching of grain and subgrains boundaries, which are the nucleation centers for precipitates of rare-earth metals rich phases.

Fig. 4 shows the microstructures of the WE43 alloy after homogenization and after HPT at room temperature, 200 °C and 300 °C. The alloy structure after homogenization consists of equiaxed grains of magnesium solid solution with an average size of 65 μm (Fig. 4a). HPT leads to intensive twinning within initial grains (Fig. 4b). The greatest twinning density is observed in case of HPT at room temperature. In this case, the width of deformation twins is 0.4 - 3.7 μm. After HPT at 200 °C it is 0.6 - 2.9 μm and 0.8 - 8.1 μm – after HPT at 300 °C.

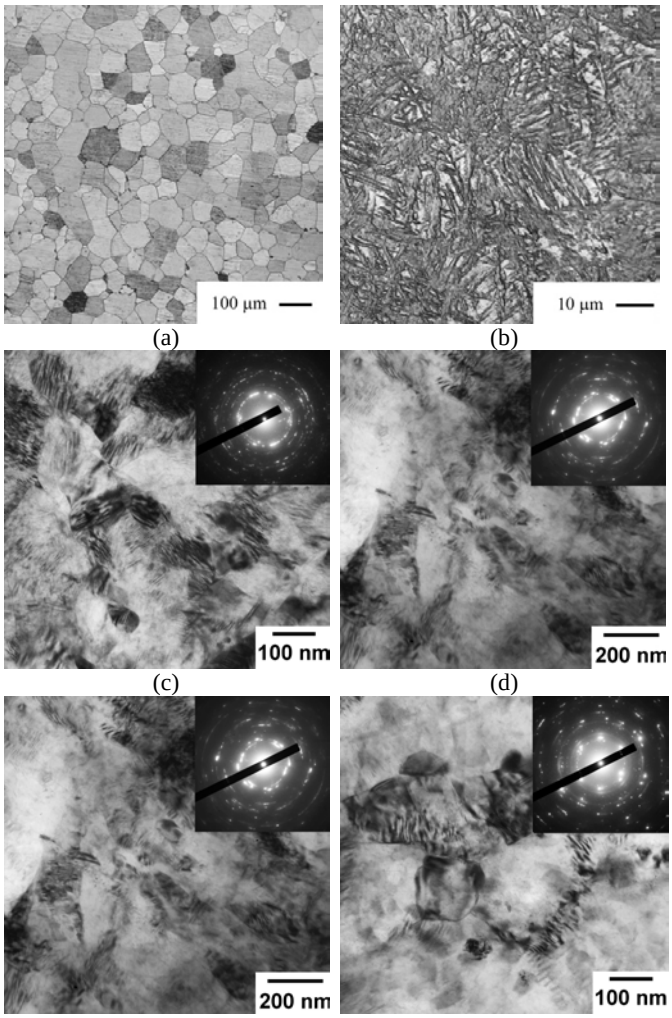

Fig. 4. Structure of WE43 alloy after homogenization (a), after HPT at room temperature (b, c), HTP at 200 °C and aging at 200 °C (2 hrs) (d), HTP at 300 °C (e) and HPT at 300 °C and aging at 200 °C (4 hrs) (f).

TEM examination showed that nanoscale grains are formed inside the twins (Fig. 4 c-f). The occurrence of high-angle boundaries is confirmed by ring-like electron diffraction patterns with a number of point reflexes. It should be noted that an increase in the deformation temperature led to an increase in the average grain size from 30 - 50 nm at room temperature to 80 - 100 nm at a temperature of 300 °C. Probably, hardening during HPT process is achieved, in a greater degree, due to grain refinement, since the maximum of hardening after HPT at room temperature corresponds to the minimum in grain size for this treatment. After subsequent aging, the grain size slightly increased to 60 - 80 nm after HPT at 200 °C and to 100 - 130 nm after HPT at a temperature of 300 °C. The strengthening precipitates are not visible in the structure after HPT and subsequent aging because of their small size, but their presence is suggested by the weak superstructure reflexes observed in the electron diffraction patterns.

Fig. 5 demonstrates the texture of the alloy before and after deformation. The texture of WE43 alloy after HPT at various deformation temperatures is sufficiently dissipated. The texture obtained after HPT is characterized by a shift of the basal poles in the radial and azimuth angles, respectively, on 20 - 30° and 45 - 50° from the center of the pole figure {00.4} (Fig. 5). The basic orientations (02-27)[3-522], (01-14)[2-1-10], (02-27)[3-522], (02-27)[5-612], (01-14)[-14.591] provide this displacement of the basal poles. The deformation temperature has a minor effect on the type of obtained texture, but the texture becomes more acute as the temperature of the HPT increases. Subsequent aging of the alloy after HPT at room temperature provides a change in the type of texture. So the basal pole on the pole figure {00.4} after aging is shifted to its center, and the orientations (02-27) [3-522] go to the orientations (0001) [10-10].

The change in texture provides a change in the activity of the basic deformation systems in the magnesium WE43 alloy: basal {0001} and prismatic {1010} slip dislocation systems in the direction <1120>, pyramidal {1122} system – in the direction <1123> and twinning {1012} – in the direction <1011>. The formed after deformation and aging texture activates the basal and pyramidal slip as well as twinning, however, it makes dislocation sliding difficult for prismatic planes. This is confirmed by orientation factors calculated for different states of the alloy (Table 1).

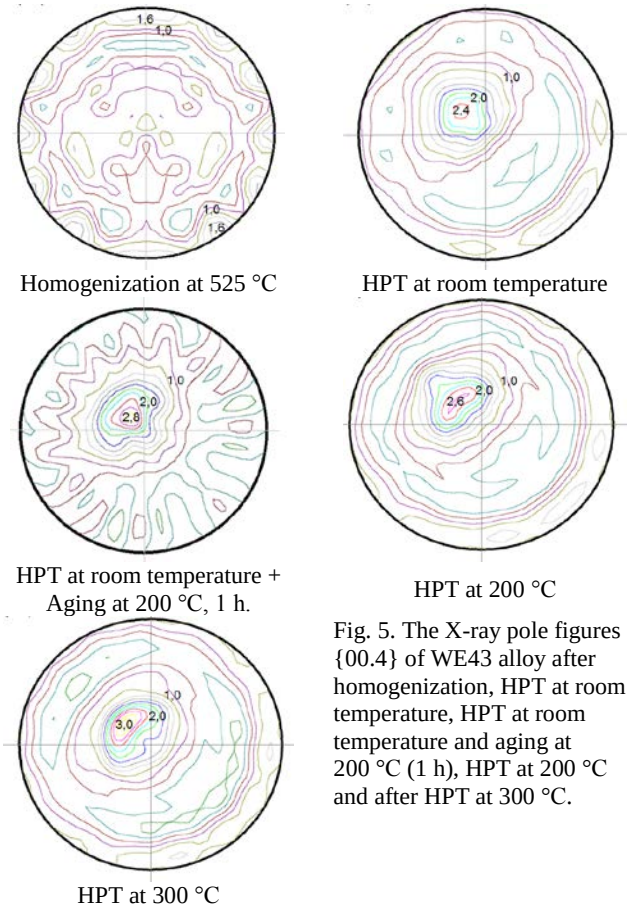

Fig. 5. The X-ray pole figures {00.4} of WE43 alloy after homogenization, HPT at room temperature, HPT at room temperature and aging at 200 °C (1 h), HPT at 200 °C and after HPT at 300 °C.

Table 1. The orientation factors for the different deformation systems of WE43 alloy

Treatment	Basal	Prismatic	Pyramidal	Twinning
HPT at 20 °C	4.800	6.031	5.210	5.540
HPT at 20 °C + Aging at 200 °C for 1 hour	4.864	6.183	4.936	5.129
HPT at 200 °C	4.749	5.920	5.131	5.407
HPT at 300 °C	4.735	6.296	4.898	5.061

Presumably the texture change after aging can be caused by the release of disperse metastable phases rich in rare earth metals, which, being coherent with the matrix of magnesium solid solution,

are released in certain planes, orienting the new ones formed as a result of the recrystallization of the grain.

4. Conclusions

1. The refinement of the structure of the WE43 alloy after the HPT occurs predominantly by deformation twinning. However, a partially nanocrystalline structure with a grain size of 30 - 100 nm is formed inside the deformation twins. Aging after HPT leads to grain growth up to 130 nm.
2. As a result of HPT at all deformation temperatures, a displaced basal texture is formed, which becomes more acute with an increase in the deformation temperature. The subsequent aging of the alloy after HPT at room temperature leads to a change in the type of texture
3. It was shown that HPT promotes significant hardening of WE43 alloy. The greatest hardening by the results of measuring the microhardness is achieved after torsion at room temperature, but with increasing deformation temperature, the microhardness gain decreases. Aging increases the strength according to the microhardness values.
4. The possibility of aging of the WE43 alloy after the HPT due to the decomposition of the magnesium solid solution is shown by the measurement of the electrical resistivity and microhardness. The maximum of hardening during the aging process is achieved by HPT at room temperature. It was shown that HPT significantly accelerates the decomposition of magnesium solid solution.

Acknowledgments

Part of this work relating to carrying out of high pressure torsion was funded by the Ministry of Education and Science of the Russian Federation (grant #14.A12.31.0001). Funding support of investigations of microstructure, texture and microhardness was provided by the Russian Science Foundation (project #17-13-01488).

5. Literature

[1] L. Tan, X. Yu, P. Wan, K. Yang. Biodegradable Materials for Bone Repairs: A Review // J. Mater. Sci. Technol, 2013, 29(6), 503-513.
[2] F. Witte, Y.F. Zheng, X.N. Gu. Biodegradable metals // Mater Sci Eng R, 2014, 77, 1-34.
[3] Y. Chen, Z. Xu, C. Smith, J. Sankar. Recent advances on the development of magnesium alloys for biodegradable implants: Review // Acta Biomater, 2014, 10, 4561-4573.
[4] S.R. Agnew, P. Mehrotra, T.M. Lillo, G.M. Stoica, P.K. Liaw. Texture evolution of five wrought magnesium alloys during route A equal channel angular extrusion: Experiments and simulations // Acta Mater, 2005, 53, 3135–3146.
[5] K.V. Kutniy, I.I. Papirov, M.A. Tikhonovsky, A.I. Pikalov, S.V. Sivtzov, L.A. Pirozhenko, V.S. Shokurov, V.A. Shkuropatenko. Influence of grain size on mechanical and corrosion properties of magnesium alloy for medical implants // Materwiss Werksttech, 2009, 40 (4), 242–246.
[6] Z. Kang, L. Zhou, J. Zhang. Achieving high strain rate superplasticity in Mg–Y–Nd–Zr alloy processed by homogenization treatment and equal channel angular pressing // Mater Sci Eng A, 2015, 633, 59–62.
[7] G. Cao, D. Zhang, W. Zhang, C. Qiu. Microstructure evolution and mechanical properties of Mg–Nd–Y alloy in different friction stir processing conditions // J. Alloys Compd, 2015, 636, 12–19.
[8] G. Cao, D. Zhang, F. Chai, W. Zhang, C. Qiu. Superplastic behavior and microstructure evolution of a fine-grained Mg–Y–Nd alloy processed by submerged friction stir processing // Mater Sci Eng A, 2015, 642, 157–166.
[9] N. Kumar, D. Choudhuri, R. Banerjee, R.S. Mishra. Strength and ductility optimization of Mg–Y–Nd–Zr alloy by microstructural design // Int J Plasticity, 2015, 68, 77–97.
[10] A.P. Zhilyaev, T.G. Langdon. Using high-pressure torsion for metal processing: Fundamentals and applications // Prog Mater Sci, 2008, 53, 893–979.
[11] K. Edalati, A. Yamamoto, Z. Horita, T. Ishihara. High-pressure torsion of pure magnesium: Evolution of mechanical properties, microstructures and hydrogen storage capacity with equivalent strain // Scr Mater, 2011, 64 (9), 880–883.
[12] X.G. Qiao, Y.W. Zhao, W.M. Gan, Y. Chen, M.Y. Zheng, K. Wu, N. Gao, M.J. Starink. Hardening mechanism of commercially pure Mg processed by high pressure torsion at room temperature // Mater Sci Eng A, 2014, 619, 95–106.
[13] P. Serre, R. B. Figueiredo, N. Gao, T. G. Langdon. Influence of strain rate on the characteristics of a magnesium alloy processed by high-pressure torsion // Mater Sci Eng A, 2011, 528 (10–11), 3601–3608.
[13] A.S.J. Al-Zubaydi, A.P. Zhilyaev, S. C. Wang, P.A.S. Reed. Superplastic behaviour of AZ91 magnesium alloy processed by high-pressure torsion // Mater Sci Eng A, 2015, 637, 1–11.
[14] S.A. Torbati-Sarraf, T.G. Langdon. Mechanical properties of ZK60 magnesium alloy processed by high-pressure torsion // Adv. Mater. Res, 2014, 922, 767–772.
[15] E.A. Lukyanova, N.S. Martynenko, I.E. Shakhova, A.N. Belyakov, L.L. Rokhlin, S.V. Dobatkin, Yu.Z. Estrin. Strengthening of an age-hardenable WE43 magnesium alloy processed by high pressure torsion // Mater Lett, 2016, 170, 5–9.
[16] D.X. Liu, X. Pang, D.L. Li, C.G. Guo, J. Wongsa-Ngam, T.G. Langdon, M.A. Meyers. Microstructural evolution and properties of a hot extruded and HPT-processed resorbable magnesium WE43 alloy // Adv Eng Mater, 2016, 19 (3), 1600698 (1-8) (doi:10.1002/adem.201600698).
[17] J.F. Nie. Precipitation and Hardening in Magnesium Alloys // Metall Mater Trans A, 2012, 43 (11), 3891–3939.